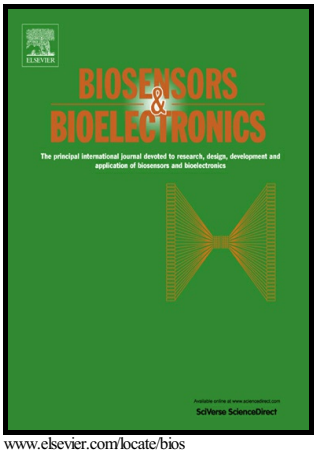

www.elsevier.com/locate/bios

A ratiometric electrochemical biosensor for the exosomal microRNAs detection based on bipedal DNA walkers propelled by locked nucleic acid modified toehold mediate strand displacement reaction

Jing Zhang, Liang-Liang Wang, Mei-Feng Hou, Yao-Kun Xia, Wen-Hui He, An Yan, Yun-Ping Weng, Lu-Peng Zeng, Jing-Hua Chen

PII: S0956-5663(17)30717-0
DOI: https://doi.org/10.1016/j.bios.2017.10.050
Reference: BIOS10075

To appear in: *Biosensors and Bioelectronic*

Received date: 21 September 2017
Revised date: 23 October 2017
Accepted date: 26 October 2017

Cite this article as: Jing Zhang, Liang-Liang Wang, Mei-Feng Hou, Yao-Kun Xia, Wen-Hui He, An Yan, Yun-Ping Weng, Lu-Peng Zeng and Jing-Hua Chen, A ratiometric electrochemical biosensor for the exosomal microRNAs detection based on bipedal DNA walkers propelled by locked nucleic acid modified toehold mediate strand displacement reaction, *Biosensors and Bioelectronic,* https://doi.org/10.1016/j.bios.2017.10.050

A ratiometric electrochemical biosensor for the exosomal microRNAs detection based on bipedal DNA walkers propelled by locked nucleic acid modified toehold mediate strand displacement reaction

Jing Zhang[a], Liang-Liang Wang[b], Mei-Feng Hou[a], Yao-Kun Xia[b], Wen-Hui He[b], An Yan[b], Yun-Ping Weng[b], Lu-Peng Zeng[b], Jing-Hua Chen[b*]

[a]College of Life Sciences, Fujian Agriculture and Forestry University, Fuzhou, Fujian Province 350002, P R China.

[b]Department of Pharmaceutical Analysis, The School of Pharmacy, Fujian Medical University, Fuzhou, Fujian Province 350108, P. R. China.

*Corresponding author. E-mail: cjh_huaxue@126.com (J. H. Chen).

Abstract

Sensitive and selective detection of microRNAs (miRNAs) in cancer cells derived exosomes have attracted rapidly growing interest owing to their potential in diagnostic and prognostic applications. Here, we design a ratiometric electrochemical biosensor based on bipedal DNA walkers for the attomolar detection of exosomal miR-21. In the presence of miR-21, DNA walkers are activated to walk continuously along DNA tracks, resulting in conformational changes as well as considerable increases of the signal ratio produced by target-respond and target-independent reporters. With the signal cascade amplification of DNA walkers, the biosensor exhibits ultrahigh sensitivity with the limit of detection (LOD) down to 67 aM. Furthermore, owing to the background-correcting function of target-independent reporters termed as reference reporters, the biosensor is robust and stable enough to be

applied in the detection of exosomal miR-21 extracted from breast cancer cell lines and serums. In addition, because locked nucleic acid (LNA) modified toehold mediate strand displacement reaction (TMSDR) has extraordinary discriminative ability, the biosensor displays excellent selectivity even against the single-base-mismatched target. It is worth mentioning that our sensor is regenerative and stable for at least 5 cycles without diminution in sensitivity. In brief, the high sensitivity, selectivity and reproducibility, together with cheap, make the proposed biosensor a promising approach for exosomal miRNAs detection, in conjunction with early point-of-care testing (POCT) of cancer.

Keywords: Ratiometric electrochemical biosensor; Exosomal miRNAs; Bipedal DNA walker; Locked nucleic acid; Toehold mediate strand displacement reaction.

1. Introduction

MicroRNAs (miRNAs), a class of single-stranded non-coding RNA molecules consisting of about 20~24 nucleotides, can act as either tumor suppressors or oncogenes in tumorigenesis (Esquela-Kerscher et al., 2006), and their expression signatures can classify human cancers, including breast cancer, lung cancer, ovarian cancer and so on. Therefore, miRNAs have been recognized as potential diagnostic biomarkers for human cancer. However, the quantity and stability of free miRNAs in biological fluids are rather limited, which impedes their further application in clinical diagnosis. Surprisingly, it is reported that circulating miRNAs presented in exosomes, small saucer-like membrane vesicles ranging approximately from 30-100 nm in diameter, are extraordinarily stable due to the protection of exosomes against RNase activity and shear stresses from the surrounding environment (Zhang et al., 2015). Furthermore, exosomes, which extensively exist in most body fluids, such as blood,

urine, breast milk, and semen, are numerous in quantity and very easy to obtain non-invasively (Vojtech et al., 2014). In addition, massive experimental evidence has confirmed both miRNAs contained in exosomes and free miRNAs have a close correlation in the diagnosis of human cancers (Taylor et al., 2008; Rabinowits et al., 2009; Skog et al., 2008; Friel et al., 2010). All above properties enable exosomal miRNAs to be promising and meaningful biomarkers allowing for non-invasive diagnosis of cancers.

Up to now, the most common exosomal miRNAs assay is PCR-based method, which requires a series complicated procedures including miRNAs isolation, cDNA synthesis, and real-time PCR analysis. Obviously, this time-, labor-, and cost-consuming technique is not appropriate for the large scale of cancer screening. By contrast, some PCR-free methods based on fluorescent molecular beacons (Lee et al., 2015) or localized surface plasmon resonance (Joshi et al., 2015) had been developed for simple and fast, or even simultaneous detection of multiple miRNAs (Lee et al., 2016). However, either the sensitivity or reproducibility needs further improvements for clinical applications.

To raise the assay sensitivity to attomolar concentration, a large variety of signal amplification methods have been explored. In particular, DNA walkers, a kind of nanoscale molecular devices fueled by protease, nuclease, deoxyribozyme or light (Cha et al., 2015; You et al., 2012), can “walk” continuously along precisely designed one-, two- or three-dimensional DNA tracks, giving rise to a cascade signal enhancement. For example, Ji et al. proposed a binding-induced DNA walker-assisted signal amplification for highly selective electrochemical detection of protein (Ji et al. 2017). Chen et al. developed an electrochemiluminescence method based on a restriction enzyme-powered autonomous DNA walking machine for highly sensitive

DNA detection down to 0.19 pM (Chen et al., 2015a). Qu et al. designed a stochastic DNA walker autonomously moving on a spherical nucleic acid-based 3D track to detect as low as 10 fM target DNA (Qu et al., 2017). However, the above DNA walkers propelled by enzyme-mediated hydrolysis were based on burnt-bridge mechanism, where DNA tracks are disposable and will break into a large amount of short DNA sequences once DNA walkers passed through, resulting in enormous cost-, time-, and labor-consuming. Besides, enzyme it has some weaknesses, such as high cost, high dependency on external environment (temperature, pH, humidity, etc.) and low stability (Chen et al., 2015b). More importantly, some above DNA walkers with only one leg may jump out of the reaction system before they can reattach to another DNA track, leading to fewer numbers of steps, along with lower efficiency of signal amplification. Surprisingly, based on TMSDR mechanism, Jung et al. proposed a stochastic DNA walker moving over a micro-particle surface without enzyme and ruining of DNA tracks for more than 30 continuous steps (Jung et al., 2016). If this kind of DNA walker can be applied in the fabrication of sensitive electrochemical biosensors, the assay sensitivity would be dramatically improved for direct detection of exosomal miRNAs in clinical real samples. Together with the unique characteristics of the electrochemical biosensor, such as simple, economic, portable and fast responsive, a promising reusable biosensor for POCT purpose can be exploited. However, electrochemical biosensors are often troubled with lower reproducibility and reliability especially for a direct determination in unprocessed clinical samples due to unavoidable changes in sensing interface, DNA assembly density and nonspecific degradation/dissociation. To solve this problem, several ratiometric methods based on dual-reporter mechanism were proposed. Unlike the previous assay using electrochemical absolute values of a single reporter, these

methods measured relative signals yielded by two redox reporters termed as target-responsive and drift-correcting reference reporter, resulting in lower background variations and higher stability and accuracy (Du et al., 2014; Li et al., 2016; Xiong et al., 2015; Deng et al., 2017; Jin et al., 2017; Pu et al., 2017).

In addition, considering multiple components in clinical real sample, a great deal of methods have been used to improve the selectivity of the electrochemical biosensors, including Y junction DNA probe, enzyme-induced cleavage reaction, 2'-deoxyinosine, TMSDR etc. (Zhang et al., 2009; Zhang et al., 2010; Zhang et al., 2016). Particularly, LNA known as bridged nucleic acids modified DNA probe can largely increase the melting temperature (Tm) difference between complementary duplex and mismatched one, as well as the discriminative ability for mismatched targets. Specially, Olson et al. integrated LNA with strand displacement reaction, gaining the increasement of the ratio of the invading rate/the leakage rate constant and the reduction of the background signal (Olson et al., 2017). Wu et al. utilized the lipoplex nanoparticles containing LNA modified molecular beacons to detect exosomal miR-21, enhancing the structural stability and avoiding false positive signal (Wu et al., 2013). The unique advantages enable LNA to be an excellent tool for single nucleotide polymorphism (SNP) discrimination even against a single base difference (Zhang et al., 2014; Chen et al., 2008).

Inspired by the above findings, a ratiometric electrochemical biosensor based on bipedal DNA walkers propelled by LNA modified TMSDR was developed in this paper. At the same time, miR-21, which has been found to be up-regulated in breast cancer (Iorio et al., 2005), lung cancer (Yanaihara et al., 2006) and chronic lymphocytic leukemia (Fulci et al., 2007), was used to test its performance. As illustrated schematically in Scheme 1, once miR-21 is isolated from breast cancer cell

derived exosomes, the two-footed DNA walkers previously attached to magnetic beads (mbs), go into free and "walk" continuously along hairpin DNAs formed "tracks" driven by TMSDR. In theory, one DNA walker can give rise to the conformational changes of all hairpin DNA tracks, resulting in considerable signal amplification. Meanwhile, there are little byproducts generated during the whole "walking" process, leading to less non-specific absorption as well as lower background signals. Therefore, the proposed sensor possesses ultrahigh sensitivity and can detect as low as 67 aM target miRNAs. Compared with the single "leg" DNA walker which may easily drift away from tracks, the bipedal walker exhibits higher signal amplification efficiency because its double "legs" would make it persist on DNA tracks for a longer time. Furthermore, on account of using a target-irrelevant signal reporter as a reference to correct the background drift, this ratiometric biosensor is stable and accurate enough to be applied for the direct detection of miR-21 in exosomes extracted from breast cancer cell lines and serum. In addition, the method shows little cross hybridization even at the single-base-mismatched level due to the excellent discriminative ability of LNA and TMSDR. As far as we know, this is the first attempt to combine DNA walker and rational electrochemical assay together for exosomal miRNAs detection, which may represent a promising path toward sensitive, reliable and economic early POCT of cancer.

2 Experimental section

2.1. Reagents and apparatus

HPLC-purified miRNAs, were purchased from Takara Biotechnology Co., Ltd. (Dalian, China). All DNA oligonucleotides were synthesized by Sangon Biotech Co. (Shanghai, China), and their base sequences were illustrated in Table S1. The

concentrations were quantified by OD260 based on their individual absorption coefficients. Streptavidin-modified magnetic beads (mbs, 10 mg·mL^{-1}) were obtained from Dynal Biotech ASA (Oslo, Norway). Human breast cancer cell line MCF-7 was purchased from China Center for Type Culture Collection in Shanghai. Fetal bovine serum (FBS), roswell park memorial institute (RPMI), phosphate buffer solution (PBS) and penicillin-streptomycin were purchased from Hyclone. Insulin was purchased from Novo Nordisk. Exosomal protein lysis buffer was purchased from Weihui Biotechnology Co., Ltd (Beijing, China). Pierce BCA Protein Assay Kit was purchased from Thermo Fisher Scientific. SDS-PAGE gel preparation kit, paraformaldehyde and glutaraldehyde were purchased from Beijing solarbio sciences & technology Co., Ltd (Beijing, China). Polyvinylidene fluoride membranes (PVDF) were purchased from Beijing Dingguo Changsheng Biotechnology Co., Ltd (Beijing, China). Tween 20 and 20×TBS were purchased from Sangon Biotech Co., Ltd (Shanghai, China). CD63 antibody and anti-CD63 antibody were purchased from Abcam. Exosomes antibodies, array & ELISA kit were purchased from System Biosciences (SBI). TRIzol was purchased from Beyotime. MiScript Ⅱ RT Kit and miScript SYBR Green PCR Kit were purchased from Qiagen. All the other chemicals were analytical grade and purchased from Sinopharm Chemical Reagent Co., Ltd (Shanghai, China). All aqueous solutions were prepared with Milli-Q water (18 MΩ).

The ultracentrifuge was Beckman Optima XPN-100 (BEKMAN, U.S.A.). The transmission electron microscopy (TEM) images were performed on a JEM-2010 microscope (JEOL Ltd., Japan). The images of proteins were obtained using Bio-Rad

ECL detecting system (Bio-Rad, U.S.A.). Enzyme-linked immunosorbent Assay (ELISA) was performed on Multiskan GO microplate spectrophotometer (Thermo Fisher Scientific, U.S.A.). RT-qPCR was performed and analyzed using MxPro-MX3000P software (Agilent Technologies, U.S.A.). The fluorescence spectra were recorded with a Cary Eclipse fluorescence spectrometer (Agilent Technologies). The differential pulse voltammetry (DPV) and electrochemical impedance spectroscopy (EIS) measurements were carried out on CHI660E analyzer (Shanghai Chenhua Instrument Co., Ltd, China).

2.2. Cell culture and exosomes isolation

MCF-7 cells were cultured in RPMI containing 10 % FBS, 1 % penicillin and streptomycin, then MCF-7 cells (1.0×10^8 cells) were cultured in RPMI containing 5 % FBS (exosomes depleted) for 48 h. Subsequently, exosomes were isolated from the above cell culture medium using the "gold standard" ultracentrifugation method with some slight changes (Théry et al., 2006). To be brief, the cell culture medium was centrifuged at 300 g for 10 min, 2000 g for 15 min and 11,000 g for 45 min to remove intact cells, dead cells, cells debris, protein and so on. Finally, the supernatant was centrifuged at 110,000 g for 3 h to acquire sediment exosomes, which were then resuspended in PBS and stored in -80 ℃ for later use.

2.3. Exosomes counting by ELISA

The number of exosomes was quantified by Exosomes Antibodies, Array & ELISA Kits (SBI). Briefly, the isolated exosomes were added and incubated at 37 ℃ overnight in the microtiter plate provided in the kit. After three washes with washing

buffer, specific rabbit anti-human CD63 antibody (System Biosciences) was added at room temperature and incubated for 1 h. After washing, the plate was incubated with HRP-conjugated goat anti-rabbit antibody (SBI) for 1 h. After the final washing, the reaction was performed with super-sensitive 3, 3', 5, 5'-tetramethylbenzidine (TMB) substrate followed by blocking with a stop buffer. Finally, the optical densities were recorded at 450 nm using Multiskan GO microplate spectrophotometer (Thermo Fisher Scientific, U.S.A.).

2.4. Transmission electron microscopy (TEM)

10 μL drops of the mixture of purified exosomes and 4 % paraformaldehyde in PBS were absorbed to formvar carbon-coated grids for 20 min. Then, exosomes were fixed in 4 % glutaraldehyde for 5 min and washed three times with deionized water. The grids were negatively stained with 1 % aqueous uranyl acetate for 5 min. After drying, the samples were visualized using JEM-2010 microscope (JEOL Ltd., Japan).

2.5. Western blot analysis of exosomal protein

Cells and exosomes were lysed in RIPA buffer (Beyotime Biotechnology) and Exosomal Protein Lysis Buffer (Weihui, China), respectively. And the total protein concentrations were quantified using the BCA assay. Then, the known concentration proteins were boiled at 98 ℃ for 5 min to facilitate denaturation. Next, the exosomal proteins were separated by 12 % SDS-polyacrylamide gel eletrophoresis (SDS-PAGE) in electrophoretic buffer (25 mM Tris, 192 mM glycine, 0.5 % SDS) at 80 V for 30 min and 100 V for 1 h. After that, the gels were transferred to polyvinylidene fluoride membranes (PVDF) that need activation with methanol in Towbin transfer buffer (25

mM Tris, 192 mM glycine, 20 % methanol) at 300 mA for 1 h. After blocking with 5 % non-fat powdered milk in TBST buffer (1×TBS containing 0.05 % Tween 20, pH 7.4) for 2 h, the PVDF membranes were incubated with 200 µl drops of rabbit anti-human CD63 antibody (Abcam) solution overnight at 4 ℃. Subsequently, the blots were incubated with HRP-conjugated goat anti-rabbit antibody at room temperature for 1 h (Abcam). Finally, an enhanced chemiluminescence reagent (Thermo Fisher Scientific) was used to visualize the immunoreactive bands, and the images were obtained using an ECL detecting system (Bio-Rad, U.S.A.).

2.6. RNA isolation, reverse transcription and PCR analysis of the exosomes

Exosomal RNA was isolated using TRIzol reagent according to the manufacturer's protocol. The concentrations of RNA were quantified by NanoDrop ND-2000 (Thermo Scientific). Total RNA was converted to cDNA using miScript II RT Kit (Qiagen) that contained 5×miScript HiSpec Buffer, 10×miScript Nucleics Mix, RNase-free water and miScript Reverse Transcriptase Mix according to manufacturer's protocol. Then the prepared solution was incubated at 37 ℃ for 1 h, and 95 ℃ for 5 min. PCR assays were performed using miScript SYBR Green PCR Kit and the PCR mixture included 10 µL of 2×QuantiTect SYBR Green PCR Master Mix, 2 µl of 10×miScript Universal Primer, 2 µL of 10×miScript Primer Assay, and 4 µL of RNase-free water. Thermocycler protocol was as follows: 95 ℃ for 15 min as the initial activation step, followed by 40 cycles of 94 ℃ for 15 s, 55 ℃ for 30 s, 70 ℃ for 30 s. The reactions were performed on Mx3000P machine (Agilent Technologies, U.S.A.) and threshold cycle (CT) data were collected with MxPro-Mx3000P

software.

2.7. The fabrication of the electrochemical biosensor and its application in miR-21 detection

2.7.1 DNA self-assembly on the mbs surface

According to the direction of Dynal Biotech ASA, under a magnetic field, a volume of 10 μL streptavidin coated mbs were washed with Tris-EDTA buffer (10 mM Tris, 1.0 mM EDTA, 0.01 % Tween 20 and 1 M $NaNO_3$, pH 7.5) for three times and resuspended in the same buffer containing 10 μL of 5 μM LNA labeled capture probe (L-Cp). After incubation for 1 h at 37 ℃ with gentle mixing, L-Cp/mbs were separated by a magnet and washed three times with the same buffer. Then 10 μL of 10 μM DNA walkers were added into L-Cp/mbs system at 25 ℃ for 1 h, followed by magnetic separation to remove the excess DNA walkers in the supernatant. Finally, the obtained DNA walker/ L-Cp/mbs were re-dispersed in Tris-EDTA buffer after washing three times with the same buffer.

2.7.2. DNA walker's release from mbs through miR-21 induced TMSDR

Different concentrations of miR-21 or exosomal extraction as described in 2.6 were added to the above prepared DNA walker/L-Cp/mbs to react for 40 min. After magnetic separation, the supernatant was collected and stored at 4 ℃. At the same time, FAM-labeled DNA walkers were used to verify the releasing feasibility of DNA walkers from mbs. That is, after the same process mentioned above, the resulting solutions were transferred to quartz fluorescence cuvettes (4 mm×10 mm; Sub-micro, 50 μL) and determined by fluorescence spectrum in the excitation wavelength

(λ_{ex}=490) at room temperature with 5 nm slit and 650 V of photoelectric multiplier (PMT).

2.7.3 Fabrication of the sensor

As shown in Scheme 1, the gold electrode (GE) was firstly polished with 0.3 μm and 0.05 μm alumina slurries to obtain a mirror-like surface, then treated with ultrasonic in deionized water and ethanol for 3 min, respectively. After rinsed with water and dried under a stream of nitrogen gas, the GE was scanned through cyclic voltammetry (CV) in 0.5 M H_2SO_4 until curve is stable. CV scanning potential varied from -0.35-+1.5 V, and the quiet time, scan rate and sample interval were 2 s, 0.1 V/s and 1 mV, respectively. Then, 2.5 μl of 1 μM methylene blue (MB) modified hairpin probes 1 (MB-H1) in Tris buffer (20 mM Tris, 140 mM NaCl, 5 mM KCl, pH 7.5) was dropped on the pre-cleaned GE surface for 1 h at room temperature to form MB-H1/GE. After washing with deionized water, MB-H1/GE was immersed in 2 mM MCH for 1 h to remove nonspecific adsorption of DNA. Next, the magnet processed supernatants containing DNA walkers were spread on the surface of MCH/MB-H1/GE and incubated for 1 h at 37 ℃. At last, 2.5 μl of 0.5 μM ferrocene (Fc) labeled hairpin probe 2 (Fc-H2) in the same Tris buffer was used to initiate walking of DNA walkers on the GE for 1 h.

2.7.4 Electrochemical detection

The electrochemical performance of the sensor was investigated by differential pulse voltammetry (DPV) in the above-mentioned Tris buffer. DPV measurement conditions were as follows: scanning potentials range from -0.40-+0.60

V, potential step of 5 mV, pulse amplitude of 50 mV, pulse width of 50 ms and a pulse period of 200 ms. Electrochemical impedance spectroscopy (EIS) was also used to mornitor the whole process of the sensor fabrication with a execution time of 2 s, an initial potential of 0.21 V and an amplitude of 0.005 V by scanning frequency range from 1~100000 Hz in 5.0 mM $K_3[Fe(CN)_6]/K_4[Fe(CN)_6]$ (1:1) solution containing 0.1 M KCl. All electrochemical experiments were performed with a conventional three-electrode system comprising the above mentioned GE, a platinum wire auxiliary electrode, and an Ag/AgCl reference electrode.

3. Results and discussion

3.1. Experimental principle of the ratiometric electrochemical biosensor

As shown in scheme 1, a DNA walker consists of two catalyst domains as its double “legs” and a linear domain as “body”. DNA tracks are built by immobilizing MB-H1 on a GE surface through Au-S bond. MB can act as a drift-correcting reference reporter due to the constant distance from the electrode surface. Initially, the “body” of DNA walker hybridizes with partially complementary L-Cp, which is previously immobilized on mbs and labeled with LNA at the toehold for higher discriminative ability, to form a duplex DNA structure (DNA walker/L-Cp/mbs) in a tube. Upon addition of miR-21 extracted from exosomes, it bands with L-Cp together through TMSDR, while releasing DNA walker freely. After magnetic separation by a magnet placed under the tube, DNA walkers contained in the supernatant are extracted and then dropped onto the electrode surface to hybridize with MB-H1 by its “leg”, leaving a new toehold on MB-H1 exposed. Subsequently, the additional Fc-H2

bands with MB-H1 through TMSDR to form H1:H2 duplex, leading the walker to move into another cycle. N cycles later, a vast majority of Fc approach the electrode surface, resulting in an outstanding increase of the electrochemical signal ratio of Fc to MB. By recording this ratio, target miR-21 can be quantified accurately and specifically.

3.2. The feasibility of the biosensor

3.2.1 Releasing feasibility of the bipedal DNA walker

To demonstrate the releasing feasibility, the bipedal DNA walker was modified with fluorescein (FAM) at its 3' end to monitor the releasing process by fluorescence spectrometry. Initially, FAM-labeled DNA walkers hybridize with L-Cp immobilized on mbs to form DNA walker/L-Cp/mbs in a tube. If the DNA walker could be released from mbs effectively, the supernatant would display a strong fluorescent signal after separation by a magnet placed under the tube. On the contrary, the supernatant reveal negligible fluorescence. Therefore, the releasing feasibility of the bipedal DNA walker can be investigated by recording fluorescent intensity of the supernatant post-magnetic separation. As depicted in Figure 1, the supernatant shows little response compared with the control signal (curve a) after the addition of 100 nM non-complementary target (NCT, curve b) or single base mismatched target (SMT, curve c), while a notable enhancement upon the addition of miR-21 (T, curve d). This phenomenon confirms the DNA walker can be released through TMSDR with miR-21, and more importantly, this releasing reaction possesses extraordinary selectivity toward miR-21 even against single base mismatched target, which may ascribe to the

high discriminative ability of LNA and TMSDR.

3.2.2 Walking feasibility of the DNA walker

The feasibility of the bipedal DNA walker moving along DNA tracks was confirmed by DPV to investigate different modified electrodes. Figure S1 shows, the MCH/MB-H1/GE has a single oxidation peak of MB at about -0.20 V (curve a). When incubated with H2, there is no obvious change because MB-H1 and Fc-H2 are kinetically trapped (curve b). Likewise, the current intensity of the MCH/MB-H1/GE dipped into magnet-processed supernatant containing DNA walkers is close to the background signal owing to the constant distance of MB from the GE surface before and after the formation of H1-walkers duplex (curve c). However, upon immersed in magnet-processed supernatant and Fc-H2, MCH/MB-H1/GE exhibits a sharp increase of Fc peak at 0.36 V, accompanied by a negligible change of MB peak (curve d). Such a change in current intensity indicates MB-H1 and Fc-H2 can hybridize with each other if and only if the DNA walker coexists with this two hairpin DNA. As the incubation time increases, the Fc signal also increases since the continuous walking of bipedal DNA walkers propelled by TMSDR in the presence of Fc-H2 cause more and more Fc near to the GE surface (curve e). The results showed here demonstrate the walking feasibility of the DNA walker.

A further evidence of the walking feasibility of the bipedal DNA walker was investigated by EIS, which can reflect interfacial property of the surface modified electrode by the electron transfer resistance (Rct) as well as the diameter of the semicircle portion in the EIS figure (Patra et al., 2015). That is, the larger the diameter,

the stronger the Rct value. As shown in Figure S2, the bare GE exhibits a nearly straight line (curve a), indicating a very fast electron transfer process of $[Fe(CN)_6]^{3-/4-}$. After modification of MB-H1, Rct increases dramatically (3393 Ω, curve b) because negative charged phosphate backbones keep $[Fe(CN)_6]^{3-/4-}$ away from the electrode surface, confirming the successful self-assembly of MB-H1 on the electrode. The value of Rct changes little when MCH/MB-H1/GE is immersed in Fc-H2 (3492 Ω, curve c), suggesting no hybridization occurring between MB-H1 and Fc-H2. And Rct exhibits only a slight increase after the hybridization of MB-H1 and DNA walkers (3872 Ω, curve d). However, the value of Rct soars to 5483 Ω (curve e) when the electrode is immersed Fc-H2 and bipedal DNA walkers, because the duplexes formed between MB-H1and Fc-H2 in the presence of DNA walkers enable more DNA attached to the electrode surface. The Rct continues to increase when prolonging the incubation time of Fc-H2 because more and more Fc-H2 hybridize with MB-H1 through TMSDR accompanied by continuous movements of DNA walkers (6569Ω, curve f). All EIS results are in a good agreement with DPV data and further verify the walking feasibility of the strategy.

3.3. Optimizations of experimental parameters

In order to achieve the best performance, experimental variables affecting the whole sensing procedure were optimized. Firstly, the parameters which play an important role on the releasing efficiency of the bipedal DNA walker, such as the incubation time of miR-21 with walker/L-Cp/mbs, the concentration of L-Cp and DNA walkers, were investigated using FAM-labeled DNA walker by fluorescence

spectrometry as described previously in 3.2.1. As shown in Figure S3, the optimal conditions are 40 min, 5 μM and 10 μM, respectively. Subsequently, the variables influencing the signal amplification of the method, including the incubation time of MCH/MB-H1/GE in the supernatant post-magnetic separation and Fc-H2, the concentration of MB-H1 and Fc-H2, were all determined. Figure S4 shows, the optimal conditions are 60 min, 1.0 μM and 0.5 μM, respectively.

3.4. The sensitivity of the biosensor

To evaluate the sensing ability of the platform toward the detection of target miR-21, a dose-response curve was monitored by DPV peak current ratio between Fc and MB (I_{Fc}/I_{MB}) under optimal conditions. As can be seen from Figure 2, the current intensity of MB keeps a constant current, and the peak current of Fc increases with the increasement of miR-21 concentrations. Likewise, I_{Fc}/I_{MB} increases with the log (concentrations) of miR-21 from 0.1 to 100.0 fM. The regression equation is I_{Fc}/I_{MB}=0.407logC+0.500 with a correlation coefficient of 0.9925, where I and C represent the current intensity and the concentration, respectively. According to the 3σ rule where σ is the standard deviation of the background signal (Qian et al., 2015), the LOD is calculated to be 67 aM when put 3σ (σ=0.007) into the regression equation as I , which is more than 1.2-, 30000-, and 300000-fold lower than that of some signal amplification strategies for exosomal miRNAs detection (Table 1). One of these strategies based on localized surface plasmon resonance (LSPR) exhibits ultrahigh sensitivity with the LOD close to our method. Nevertheless, its reproducibility is not high enough and needs further improvement. When compared with other methods for

the detection of miR-21 contained in cells and serums, the proposed sensor is also more sensitive with the LOD more than 4.5-fold lower. The data are given in Table 1.

In addition, two analogous non-ratiometric assays based on the absolute signal of Fc reporter were designed and used to detect miR-21 under the same conditions, one was signal-off and the other was signal-on method. As shown in Figure S5 (A) and Figure S5 (B), although their LOD of 87 aM and 74 aM are quite similar to that of the ratiometric biosensor, both of them display large error bars, which are ascribed to the variance of the background signal coming from different electrode areas, probe densities, cleaning procedures and so on. In short, ratiometric biosensor has obvious advantages in accuracy and reproducibility than the non-ratiometric biosensor.

3.5. The selectivity of the biosensor

In order to evaluate the specificity of the proposed biosensor, we performed a series of contrast experiments using one- and two-base mismatched miR-21 and non-complementary one. Figure 3 shows, the current signals of Fc (I_{Fc}) in the presence of all three types of mismatched miR-21 are nearly negligible compared with the background signal at about 0.36 V. However, I_{Fc} increases dramatically upon the addition of target miR-21. It is noteworthy that the peak currents of MB (I_{MB}) keep a constant current at about -0.20 V with whatever above RNAs' addition, indicating a higher uniformity/stability of the experiment conditions. The excellent specificity of the proposed approach for the single base mismatched target recognization should be ascribed to the excellent discriminative ability of LNA and TMSDR.

3.6. The reproducibility and regeneration of the biosensor

To investigate the reproducibility of the biosensor, we used identical and different batches of biosensors to analyze 1 fM miR-21 for 5 times, respectively. We observed the intra- and inter-assay coefficients of variation were 3.21 % and 4.47 %, respectively, which were lower than a vast majority of electrochemical biosensors using absolute value of a signal reporter.

In addition, the biosensor can be revived just by incubating the used electrode in 88 ℃ water for 5 min and then washing several times with deionized water. We found that the I_{Fc}/I_{MB} signal only reduced 8 % in comparison with the initial response after five cycles of the regeneration process. All above findings demonstrate the good stability and regeneration ability of this ratiometric biosensor.

3.7. Detection of miR-21 in exosomes derived from cells and real samples

To study whether this biosensor could be applied in exosomal miRNAs detection, we also quantified miR-21 in exosomes isolated from the culture medium of breast cancer cell line MCF-7 through sequential centrifugation. At first, the obtained exosomes were characterized by TEM and western blotting. As shown in Figure S6 (A), the purified exosomes have round structures with sizes varying from 30 to 100 nm, which is in agreement with the characteristics of exosomes described in the previous literature (Lee et al., 2016; Xia et al., 2017). Subsequently, western blotting was used to analyze surface membrane protein CD63. The obvious bandings in Figure S6 (B) further validate the efficacy of the separation of the exosomes. Afterwards, PCR was adopted to detect the miR-21 concentration in exosomes, in which U6 snRNA was used as an internal control (Figure S6 (C)). The template RNA was

obtained from a total of 2.04×10^{13} particles exosomes. The threshold cycle (Ct) value of miR-21 was 24.6, while that of U6 snRNA was 29.7. This result is in accordance with the previous report where the level of miR-21 in breast cancer cell-derived exosomes was up-regulated (Wickramasinghe et al., 2009). Finally, the proposed ratiometric biosensor was used to quantify exosomal miR-21 derived from either breast cancer cell line MCF-7 or non-cancer cell line CHO-K1. The results are in a good agreement with the findings of the PCR method (Figure 4A), indicating the practical value of our designed sensor in miR-21 detection. Meanwhile, it is worth noting that the concentration of exosomal miR-21 extracted from cancer cells is much higher than that from normal cells. Additionally, conforming to the relevant guidelines and regulations, we measured the concentrations of exosomal miR-21 derived from the serums of breast cancer patient and normal controls, respectively. The exosomes collection from the real samples was performed according to our previous report (Xia et al., 2017), and RNA isolation was as described in section 2.6. As Figure 4B shows, the levels of miR-21 of the breast cancer patients is 2.5-fold higher than that of the normal controls indicating the overexpression of exosomal miR-21 in breast cancer patients. The above results are in accordance with the cells analysis, which may provide great opportunities for the diagnosis of breast cancer by exosomal miR-21 detection. Furthermore, investigations for more biological samples are underway in our group to further demonstrate the real application of this biosensor in clinical analysis.

4. conclusion

In summary, an electrochemical biosensor combining merits of DNA walker, ratio assay, LNA and TMSDR is developed here for exosomal miR-21 detection. Due to the cascade signal amplification of two-footed DNA walkers, the biosensor displays ultrahigh sensitivity with the LOD down to 67 aM. Moreover, LNA and TMSDR confer excellent selectivity to the biosensor even against single-base-mismatched target. In addition, with the introduction of the target-irrelevant signal reporter as a reference, the biosensor presents extraordinary stability and reproducibility for the direct detection of miR-21 in the exosomes derived from breast cancer cells. All above superiorities, as well as other advantages originated from electrochemical biosensor, such as fast, cheap and portable make possible the proposed sensor used in developing POCT devices for early diagnosis of cancer. Future studies are required to further increase its performance. For example, the linear "body" of DNA walkers may be replaced by a nanosphere to associate more legs, giving rise to longer time and more steps of walking on the DNA tracks, along with higher sensitivity of the biosensor. And more appropriate couples of electrochemical indicators would be explored to realize simultaneous detection of multiple tumor markers, which may substantially increase the sensor's practicability for clinic diagnosis. In addition, we are considering using magnetic electrodes to integrate the procedures of exosomal capture, release, crush and detection into a coherent whole through its magnetic and electric fields. On the one hand, this improvement might dramatically simplify the fabrication process of the proposed

biosensor. On the other hand, the unavoidable loss when transferring the samples from tubes to the electrodes surface might be cut down, resulting higher sensitivity of the biosensor. In a word, we deem the approach described here as useful and attractive as a potential alternative for the early POCT diagnosis.

Acknowledgement

The authors gratefully acknowledge the financial support of National Natural Science Foundation of China (21375017), the National Science Foundation of Fujian Province (2017J07001, 2016J01042), United Fujian Provincial Health and Education Project for Tackling the Key Research .P.R. China (WKJ2016-2-30), Fujian Science and Technology Innovation Joint Found Project (2016Y9050), the Medical Elite Cultivation Program of Fujian, P. R.C (2014-ZQN-ZD-26), the National Science Foundation for Distinguished Young Scholars of Fujian Province (2013J06003), Program for New Century Excellent Talents of Colleges and Universities in Fujian Province (JA13130).

References

Cha, T.G., Pan, J., Chen, H., Robinson, H.N., Li, X., Mao, C., Choi, J.H., 2015. J. Am. Chem. Soc. 137, 9429-9437.

Chen, A., Ding, Y., Yang, Z., Yang, S., 2015b. Biosens. Bioelectron. 74, 967–973.

Chen, J., Zhang, J., Wang, K., Lin, X., Huang, L., Chen, G., 2008. Anal. Chem. 80, 8028-8034.

Chen, Y., Xiang, Y., Yuan, R., Chai, Y., 2015a. Nanoscale. 7, 981-986.

Deng, C., Pi, X., Qian, P., Chen, X., Wu, W., Xiang, J., 2017. Anal. Chem. 89, 966−973.

Du, Y., Lim, B.J., Li, B., Jiang, Y.S., Sessler, J.L., Ellington, A.D., 2014. Anal. Chem. 86, 8010−8016.

Esquela-Kerscher, A., Slack, F.J., 2006. Nat. Rev. Can. 6, 259-269.

Friel, A.M., Corcoran, C., Crown, J., O'Driscoll, L., 2010. Breast Cancer Res. Treat. 123, 613-625.

Fulci, V., Chiaretti, S., Goldoni, M., Azzalin, G., Carucci, N., Tavolaro, S., Castellano, L., Magrelli, A., Citarella, F., Messina, M., Maggio, R., Peragine, N., Santangelo, S., Mauro, F.R., Landgraf, P., Tuschl, T., Weir, D.B., Chien, M., Russo, J.J., Ju, J., Sheridan, R., Sander, C., Zavolan, M., Guarini, A., Foà, R., Macino, G., 2007. Blood. 109, 4944–4951.

Goda, T., Masuno, K., Nishida, J., Kosaka, N., Ochiya, T., Matsumoto, A., Miyahara, Y., 2012. Chem. Commun. 48, 11942-11944.

Hong, C., Baek, A., Hah, S.S., Jung, W., Kim, D.E., 2016. Anal. Chem. 88, 2999-3003.

Hong, C.Y., Chen, X., Li, J., Chen, J.H., Chen, G., Yang, H.H., 2014. Chem. Commun. 50, 3092-3295.

Iorio, M.V., Ferracin, M., Liu, C.G., Veronese, A., Spizzo, R., Sabbioni, S., Magri, E., Pedriali, M., Fabbri, M., Campiglio, M., Ménard, S., Palazzo, J.P., Rosenberg, A., Musiani, P., Volinia, S., Nenci, I., Calin, G.A., Querzoli, P., Negrini, M., Croce,

C.M., 2005. Cancer Res. 65, 7065–7070.

Jin, H., Gui, R.J., Yu, J.B., Lv, W., Wang, Z.H., 2017. Biosens. Bioelectron. 91, 523−537.

Ji, Y., Zhang, L., Zhu, L., Lei, J., Wu, J., Ju, H., 2017. Biosens. Bioelectron. 96, 201-205.

Joshi, G.K., Deitz-McElyea, S., Liyanage, T., Lawrence, K., Mali, S., Sardar, R., Korc, M., 2015. ACS. Nano. 9, 11075-11089.

Jung, C., Allen, P.B., Ellington, A.D., 2016. Nat. Nanotechnol. 11, 157-163.

Lee, J.H., Kim, J.A., Jeong, S., Rhee, W.J., 2016. Biosens. Bioelectron. 86, 202-210.

Lee, J.H., Kim, J.A., Kwon, M.H., Kang, J.Y., Rhee, W.J., 2015. Biomaterials. 54, 116-125.

Li, H., Arroyo-Currás, N., Kang, D., Ricci, F., Plaxco, K.W., 2016. J. Am. Chem. Soc. 138, 15809-15812.

Olson, X., Kotani, S., Yurke, B., Graugnard, E., Hughes, W.L., 2017. J. Phys. Chem. B. 121, 2594-2602.

Patra, S., Roy, E., Madhuri, R., Sharma, P.K., 2015. Anal. Chim. Acta. 853, 271–284.

Pu, Q., Li, J., Qiu, J., Yang, X., Li, Y., Yin, D., Zhang, X., Tao, Y., Sheng, S., Xie, G., 2017. Biosens. Bioelectron. 94, 719-727.

Qian, Y., Wang, C., Gao, F., 2015. Biosens. Bioelectron. 63, 425-431.

Qu, X., Zhu, D., Yao, G., Su, S., Chao, J., Liu, H., Zuo, X., Wang, L., Shi, J., Wang, L., Huang, W., Pei, H., Fan, C., 2017. Angew. Chem. Int. Ed. Engl. 56, 1855-1858.

Rabinowits, G., Gerçel-Taylor, C., Day, J.M., Taylor, D.D., Kloecker, G.H., 2009. Clin. Lung Cancer. 10, 42-46.

Skog, J., Würdinger, T., Van Rijn, S., Meijer, D.H., Gainche, L., Sena-Esteves, M., Curry, W.T. Jr., Carter, B.S., Krichevsky, A.M., Breakefield, X.O., 2008. Nat. Cell Biol. 10, 1470-1476.

Taller, D., Richards, K., Slouka, Z., Senapati, S., Hill, R., Go, D.B., Chang, H.C., 2015. Lab. Chip. 15, 1656-1666.

Taylor, D.D., Gercel-Taylor, C., 2008. Gynecol. Oncol. 110, 13-21.

Théry, C., Amigorena, S., Raposo, G., Clayton, A., 2006. Curr. Protoc. Cell Biol. 3.22.1-3.22.29.

Vojtech, L., Woo, S., Hughes, S., Levy, C., Ballweber, L., Sauteraud, R.P., Strobl, J., Westerberg, K., Gottardo, R., Tewari, M., Hladik, F., 2014. Nucleic Acids Res. 42, 7290-7304.

Wickramasinghe, N.S., Manavalan, T.T., Dougherty, S.M., Riggs, K.A., Li, Y., Klinge, C.M., 2009. Nucleic Acids Res. 37, 2584-2595.

Wu, Y., Kwak, K.J., Agarwal, K., Marras, A., Wang, C., Mao, Y., Huang, X., Ma, J., Yu, B., Lee, R., Vachani, A., Marcucci, G., Byrd, J.C., Muthusamy, N., Otterson, G., Huang, K., Castro, C.E., Paulaitis, M., Nana-Sinkam, S.P., Lee, L.J., 2013. Anal. Chem. 85, 11265-11274.

Xia, Y., Liu, M., Wang, L., Yan, A., He, W., Chen, M., Lan, J., Xu, J., Guan, L., Chen, J., 2017. Biosens. Bioelectron. 92, 8-15.

Xiong, E., Zhang, X., Liu, Y., Zhou, J., Yu, P., Li, X., Chen, J., 2015. Anal. Chem. 87, 7291−7296.

Yanaihara, N., Caplen, N., Bowman, E., Seike, M., Kumamoto, K., Yi, M., Stephens, R.M., Okamoto, A., Yokota, J., Tanaka, T., Calin, G.A., Liu, C.G., Croce, C.M.,

Harris, C.C., 2006. Cancer Cell. 9, 189–198.

You, M., Chen, Y., Zhang, X., Liu, H., Wang, R., Wang, K., Williams, K.R., Tan, W., 2012. Angew. Chem. Int. Ed. Engl. 51, 2457-2460.

Yu, Y., Chen, Z., Shi, L., Yang, F., Pan, J., Zhang, B., Sun, D., 2014. Anal. Chem. 86, 8200-8205.

Zhang, J., Chen, J.H., Chen, R.C., Chen, G.N., Fu, F.F., 2009. Biosens. Bioelectron. 25, 815-819.

Zhang, J., Li, S., Li, L., Li, M., Guo, C., Yao, J., Mi, S., 2015. Genomics Proteomics Bioinformatics. 13, 17-24.

Zhang, J., Wu, D.Z., Cai, S.X., Chen, M., Xia, Y.K., Wu, F., Chen, J.H., 2016. Biosens. Bioelectron. 75, 452-457.

Zhang, J., Wu, X., Chen, P., Lin, N., Chen, J., Chen, G., Fu, F., 2010. Chem. Commun. 46, 6986-6988.

Zhang, X., Zhang, J., Wu, D., Liu, Z., Cai, S., Chen, M., Zhao, Y., Li, C., Yang, H., Chen, J., 2014. Analyst. 139, 6109-6112.

Zheng, J., Ma, D., Shi, M., Bai, J., Li, Y., Yang, J., Yang, R., 2015. Chem. Commun. 51:16271-16274.

Figure Captions

Scheme 1. Schematic illustration of the ratiometric electrochemical biosensor for exosomal miR-21detection.

Figure 1. Fluorescence spectra of the supernatant post-magnetic separation with the control signal (a), the addition of NCT (b), SMT (c) and T (d), respectively. The insert is the histogram of fluorescent intensity.

Figure 2. The proposed ratiometric biosensor based on the ratio of I_{Fc}/I_{MB}. DPV curves for miR-21 detection with the concentration range from 0 to 100 fM: (a) 0, (b) 0.1, (c) 0.5, (d) 1.0, (e) 5.0, (f) 10.0, (g) 50.0, (h) 100.0 fM.

Figure 3. Selectivity of the proposed biosensor toward natural and mismatched miR-21 at the same concentrations (100 fM). (a) Blank, (b) NCT, (c) TMT, (d) SMT, (e) miR-21. The insert is the histogram of the ratio of I_{Fc}/I_{MB}. Each data point represents the average value of three independent experiments with error bars indicated.

Figure 4. The quantitative results of the proposed biosensor and PCR for the detection of exosomal miR-21 produced from (A) breast cancer cell line MCF-7 or non-cancer cell line CHO-K1 and (B) breast cancer patient serums or normal controls.

Figures:

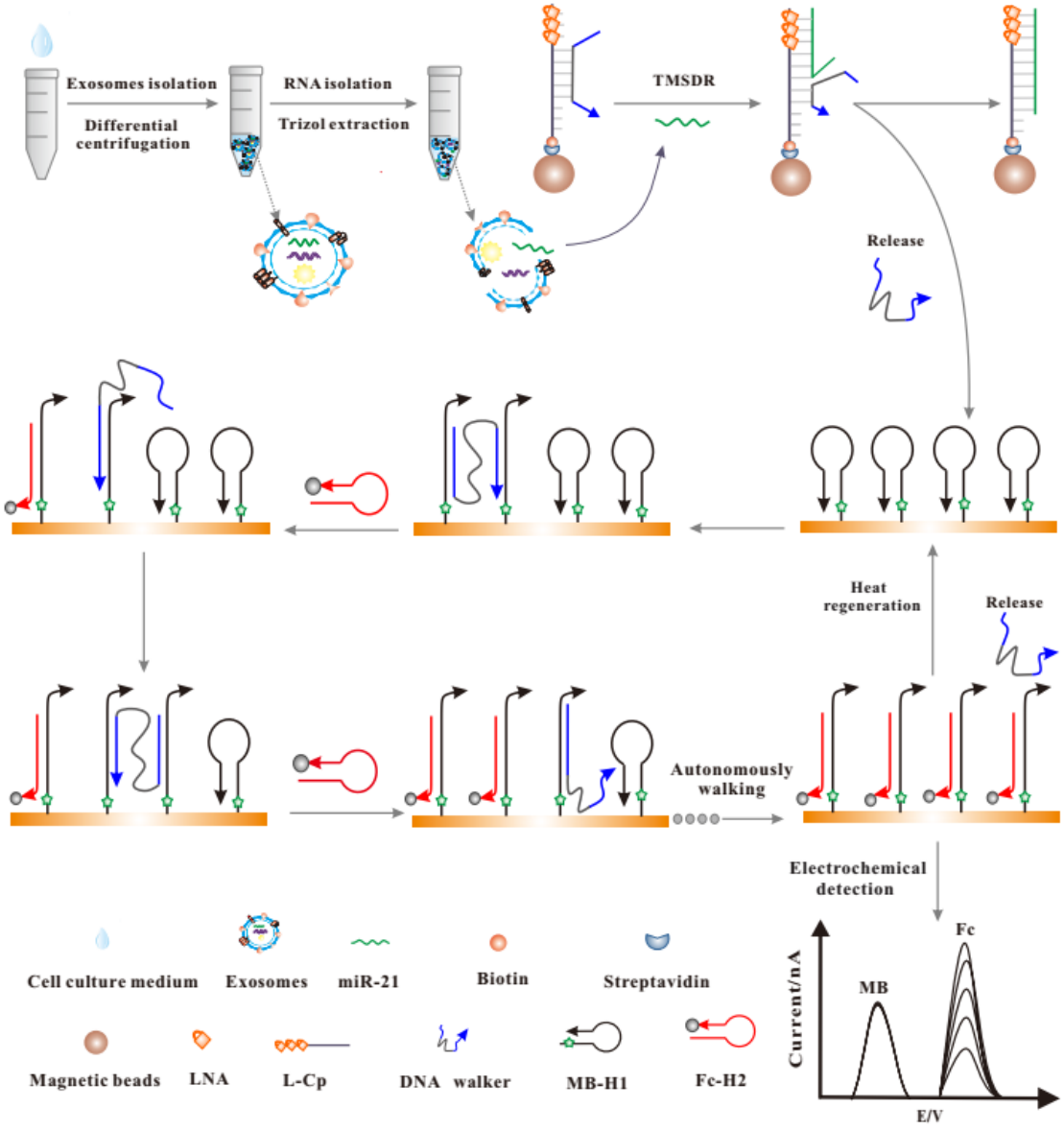

Scheme 1.

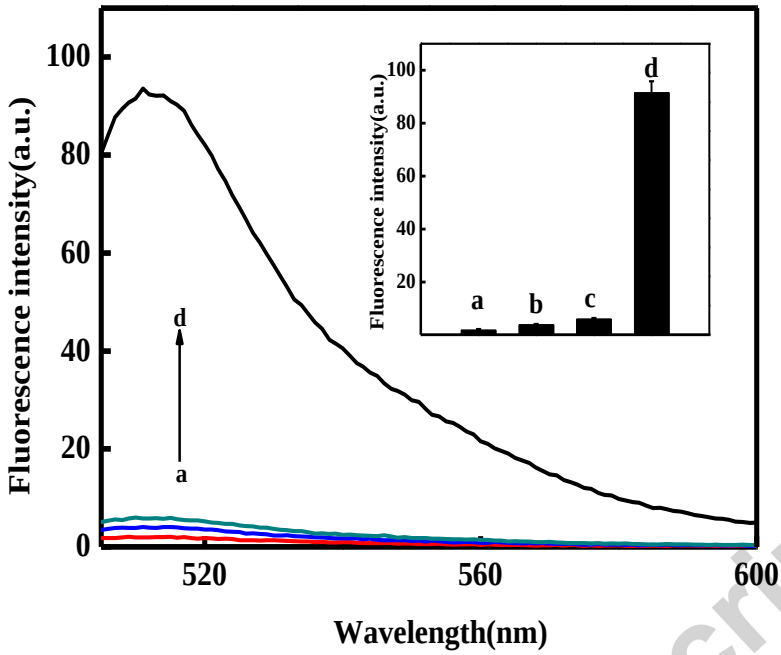

Figure 1.

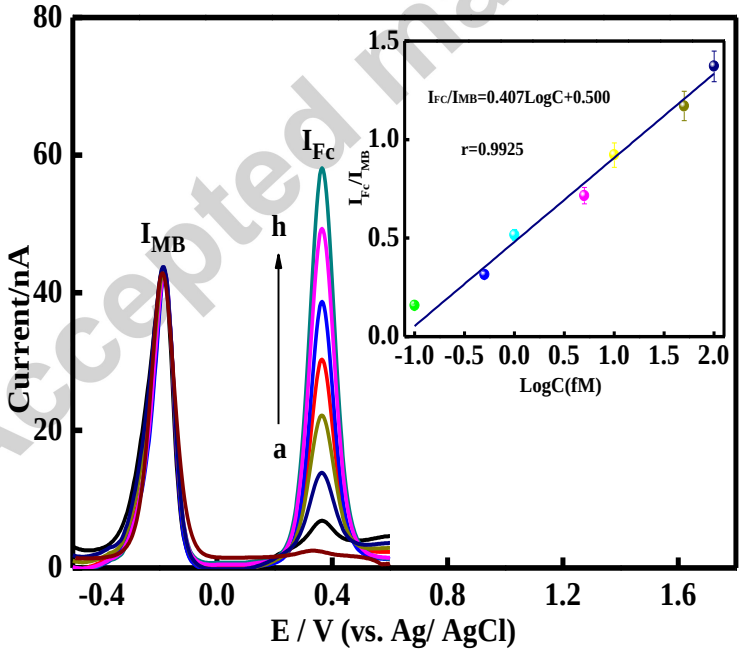

Figure 2.

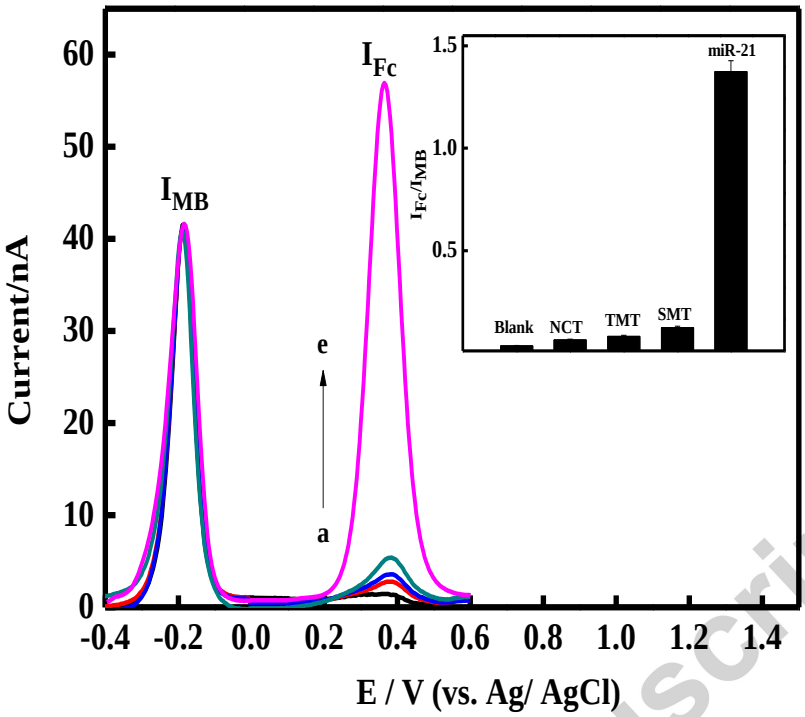

Figure 3.

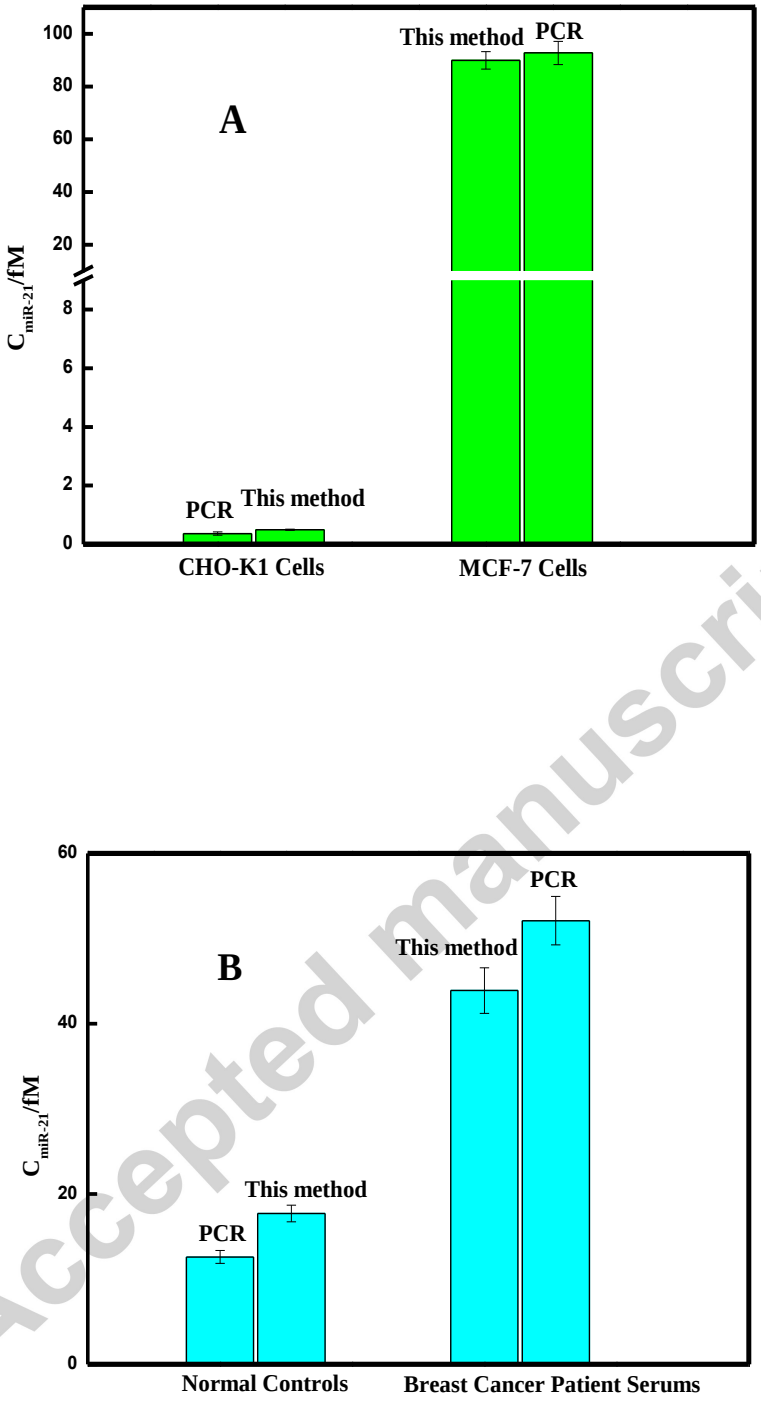

Figure 4

Table 1. Comparison with recent methods for miRNAs detection

Source		Methods and Strategies	LOD	Reference
Exosomes	miR-21	A fluorescence sensor based on single step detection in situ	Not shown	Lee et al., 2015
	miR-21	A fluorescence sensor based on simultaneous and multiplexed detection	Not shown	Lee et al., 2016
	miR-10b	A microRNA sensor based on localized surface plasmon resonance (LSPR)	83 aM	Joshi et al., 2015
	miR-550	Microfluidics chips based on surface acoustic wave (SAW) exosome lysis and ion-exchange nanomembrane RNA sensing	2 pM	Taller et al., 2015
Cells	miR-143 or miR-146a	A electrochemical sensor based on microelectrode array	~20pM	Goda et al., 2012
	miR-21	A electrochemical sensor based on arched probe mediated isothermal exponential amplification	5.36 fM	Yu et al., 2014
	miR-21	A fluorometric sensor based on isothermal gene amplification and graphene oxide	0.7 pM	Hong et al., 2016
Serum	miR-21	A fluorescence sensor based on the p19 protein-functionalized magnetic beads (PFMBs) and rolling circle amplification (RCA)	1 fM	Hong et al., 2014
	miR-21	Surface-enhanced raman spectroscopy(SERS) based on hybridization chain reaction and ions-mediated cascade amplification	0.3 fM	Zheng et al., 2015
Exosomes	miR-21	A ratiometric electrochemical biosensor based on bipedal DNA walkers and LNA modified toehold mediate strand displacement reaction (TMSDR)	67 aM	This work

Highlights

- The proposed electrochemical biosensor combining merits of the DNA walker, ratio assay, locked nucleic acid and toehold mediate strand displacement reaction possesses ultrahigh sensitivity and selectivity for exosomal miR-21 detection.
- The DNA walkers fueled by the toehold mediate strand displacement reaction are superior to the "burnt bridge" mechanism based walkers for their renewable DNA tracks.
- The ratiometric electrochemical biosensor presents extraordinary stability and reproducibility for the exosomal microRNAs detection due to a background-correcting reporter.